International Journal of Nanomedicine

Dovepress
Taylor & Francis Group

Open Access Full Text Article

ORIGINAL RESEARCH

Cardiac Homing Peptide-Functionalized Polymeric Nanoparticles Suppressing SHP1 Alleviate Acute Myocardial Infarction Injury by Promoting Efferocytosis and Inhibiting Inflammation

Qi Pan[1,*], Guihao Chen[1,*], Xiaoli Zhuang[2,*], Fei Li[3], Yuejin Yang[1]

[1]State Key Laboratory of Cardiovascular Disease, National Center for Cardiovascular Diseases, Fuwai Hospital, Chinese Academy of Medical Sciences and Peking Union Medical College, Beijing, People's Republic of China; [2]Department of Anesthesiology, Beijing Anzhen Hospital, Capital Medical University, Beijing, People's Republic of China; [3]Department of Cardiac Surgery, Beijing Anzhen Hospital, Capital Medical University, Beijing, People's Republic of China

*These authors contributed equally to this work

Correspondence: Fei Li; Yuejin Yang, Email drfeili@hotmail.com; fwyangyj@126.com

Purpose: Acute myocardial infarction (AMI) is a major global health concern worldwide. The upregulation of the CD47 on apoptotic cardiomyocytes acts as a "don't-eat-me" signal, inhibiting the clearance of apoptotic cells by macrophages (a process known as efferocytosis) via the Signal Regulatory Protein α (SIRPα)/ SH2 Domain-Containing Phosphatase 1 (SHP1) axis, leading to secondary inflammatory activation. Additionally, impairment of this process can result in insufficient macrophage polarization towards the reparative M2 phenotype. Systemic interventions targeting this axis are constrained by potential adverse effects such as promoting fibrosis, suppressing immunity, and interfering with the protective function of the axis to avoid phagocytosis of normal cells.

Methods: In this study, a poly(lactic-co-glycolic acid)@Polydopamine (PLGA@PDA) nanoparticle system was developed to deliver the SHP1 inhibitor TPI1 (NP-TPI1). The nanoparticle was modified with cardiac homing peptide (CHP) to enable heart homing (NP-TPI1/P). Raw264.7 cells and mouse AMI models were utilized to assess the pro-efferocytic, anti-inflammatory, and cardioprotective effects of the novel nanosystem.

Results: This novel nanoparticle, which is responsive to ROS and low pH, effectively inhibited SHP1 phosphorylation both in vitro and in vivo, thereby restoring timely clearance of apoptotic cells by macrophages. It also promotes M2 polarization and reduces the secondary inflammatory response. These engineered nanoparticles exhibited an enhanced capability to target infarcted lesions, and AMI mice treated with CHP-modified TPI1-loaded nanoparticles showed significantly improved cardiac performance (left ventricular ejection fraction [LVEF] of NP-TPI1/P vs PBS, 49.42±1.88 vs 31.61±2.30 [%] at day 21 post-AMI) and reduced fibrotic area (NP-TPI1/P vs PBS, 11.60±1.60 vs 25.48±1.98 [% of left ventricular]).

Conclusion: This study provides new insights into the development of novel, dual-purpose nanomedicines for post-myocardial infarction, and holds significant potential for the clinical translation of efferocytosis in cardiovascular diseases.

Keywords: SHP1, nanoparticle, myocardial infarction, efferocytosis, inflammation

Introduction

Atherosclerotic cardiovascular disease (ASCVD), particularly acute myocardial infarction (AMI), is the leading cause of premature death worldwide, accounting for over 330 million years of life lost (YLLs) annually.[1] Accumulating evidence indicates that defective efferocytosis of macrophages is a key factor in myocardial infarction injury, leading to excessive evoked and prolonged inflammation and deteriorating cardiac remodeling.[2,3] Efferocytosis refers to the process by which macrophages engulf and clear dead cells, induce the pro-repair M2 phenotype, and elevate the secretion of anti-inflammatory factors is elevated.[4,5] In infarcted hearts, impairment of efferocytosis is at least partly attributed to the

Received: 5 May 2025
Accepted: 29 July 2025
Published: 27 August 2025

Graphical Abstract

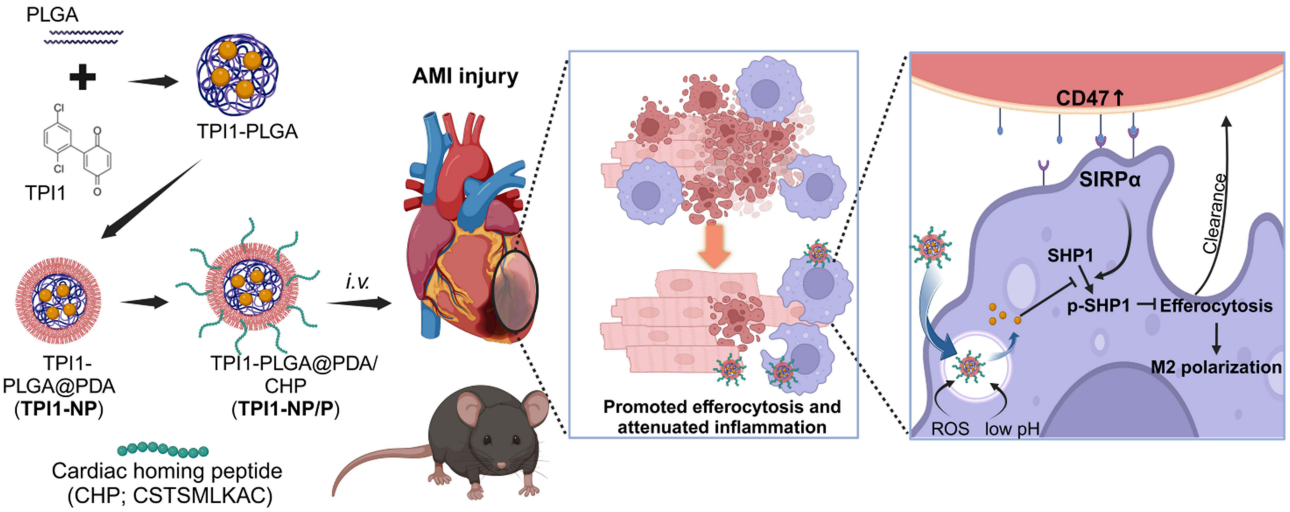

upregulation of CD47, one of the essential anti-phagocytic molecules (also known as "don't-eat-me" signals). CD47 binds to signal regulatory protein-α (SIRPα) on macrophages, thus activating Src homology 2 domain-containing phosphatase-1 (SHP1), which suppresses phagocytic function.[3,6,7] Although a series of associated therapies have been reported to attenuate acute cardiac ischemic injury,[3,6] challenges remain in clinically translating the systemic administration of inhibitors of the CD47/SIRPα/SHP1 axis (eg, Urabrelimab, NCGC00138783, and TPI1) owing to potential immunosuppressive and pro-fibrotic effects, inspiring exploration of the possibility of lesion-targeting delivery.[8,9]

The establishment of engineered nanoparticles is a promising approach to deliver drugs for the treatment of AMI, since the unmodified nanoparticles mainly accumulate in the liver and hardly reach the infarction area. Surface modifications with ligands or cardiac homing peptides (CHP), and membrane coating or hybridization are considered two well-recognized options.[10] However, the former is more conducive to clinical translation and large-scale production due to the use of stable, easily prepared reagents and the avoidance of introducing new cellular components (typically platelet, macrophage, or neutrophil membranes).[3,11,12] Functionalization with CHP, a family of peptides comprising the motif CSTSMLKAC, has been proven to significantly enhance the retention rate in hearts.[13,14]

Herein, a CHP-functionalized poly (lactic-co-glycolic acid) (PLGA)@polydopamine (PDA) nanoparticle carrying TPI1, which significantly suppressed the phosphorylation and activity of SHP1, was constructed.[15] The nanosystem is hypothesized to exhibit an increased cardiac-targeting capability, and enhanced pro-efferocytic and secondary anti-inflammatory effects in experimental AMI mouse models. This study provides insight into the development of heart-specific dual-purpose nanotherapy for AMI treatment.

Materials and Methods

All experiments were conducted following the guidelines set by the Public Health Service with approval from the Animal Care and Use Committee at Fuwai Hospital, Peking Union Medical College of Medicine (FW-2023-0026).

Preparation of Nanoparticles

TPI1-loaded PLGA@PDA (NP-TPI1) and CHP-modified NP (NP-TPI1/P) were prepared as previously described procedure.[16,17] Briefly, 100mg PLGA (50/50, 20000Da) and 5mg TPI1 were dissolved in dichloromethane (DCM, 4mL), an organic solvent. This solution was then mixed with polyvinyl alcohol (PVA, 5%) solution (25mL) and emulsified by sonication to form an oil-in-water (O/W) emulsion. The emulsion was obtained by sonication to ensure uniform distribution of PLGA and the drug. Subsequently, the emulsion was mixed with an equal volume of ddH_2O, and

the organic solvent was removed by stirring the emulsion overnight at room temperature. The unencapsulated drug and residual emulsifier were subsequently removed by dialysis to purify the nanoparticles, yielding TPI1-loaded PLGA nanoparticles. Next, the TPI1-loaded PLGA nanoparticles were dispersed in 10mM Tris-buffered solution (pH 8.5) to a concentration of 2mg/mL. Dopamine hydrochloride (2mg/mL) was then added to the dispersion in a 1:3 ratio; the solution was then stirred overnight to enable the formation of PDA layers on the nanoparticle surface. Afterwards, the mixture was then centrifuged and washed to remove unreacted material, resulting in NP-TPI1. To functionalize the surface of NP-TPI1 with CHP, the nanoparticles and the CHP (solubilized in dimethyl sulfoxide [DMSO]) were dispersed in sterile water and stirred overnight. After incubation, the nanoparticles were purified by centrifugation and washed to remove excess peptides, yielding the final NP-TPI1/P. The corresponding control particles (NP and NP/P) were prepared without the addition of TPI1. PLGA, PVA and dopamine hydrochloride were purchased from Sigma, USA.

Characterization of Nanoparticles

Transmission electron microscope (TEM) was used to obtain the images of all nanoparticles (FEI Tecnai G2 F20, FEI, USA); and dynamic light scattering was used to measure the size distribution and zeta potential of all nanoparticles using a Zetasizer Nano ZS (Malvern Nano, UK).[18] Coomassie Brilliant Blue staining was performed using a Coomassie Brilliant Blue Fast Staining solution (Solarbio, China). For drug release study, absorption at 247 nm was measured to calculate the concentration of TPI1 in solution. Loading efficiency (LE) was calculated as $(W_{Total}-W_{Free})/W_{Nanoparticle}$, where W_{Total} is the total weight of TPI1, W_{Free} is the weight of nonencapsulated/free TPI1, $W_{Nanoparticle}$ is the weight of nanoparticle. Encapsulation efficiency (EE) was calculated as $(W_{Total}-W_{Free})/W_{Total}$. To test the stability and drug release rate of nanoparticles, different particle solutions were placed in dialysis bags, and the release medium were 100 mM hydrogen peroxide (H_2O_2) solution or PBS solution (pH=7.4 or 6.8). Sampling and testing of TPI1 concentration at different time points.

Cell Culture

H9C2 cells (rodent cardiomyocyte cell line) and Raw264.7 cells (rodent monocyte/macrophage cell line) were purchased from Procell (China), and cultured in high glucose Dulbecco's modified Eagle's medium (DMEM, Gibco, USA) supplemented with 10% fetal bovine serum (FBS, 10%, Gibco) and 1% Penicillin-Streptomycin (1%, Gibco) at 37°C in a humidified chamber with 95% air and 5% CO_2.[19] H9C2 cells were used to prepare apoptotic bodies (ABs) by incubation with Staurosporine (STS, 100 nM) for 12 hours.[20] ABs were harvested by centrifugation at 1,000 *g*. For all cell experiments, ABs were administered to Raw264.7 cells at a ratio of 5:1.[21] RAW264.7 cells were seeded in confocal dishes in 6-well or 96-well plates and cultured for 24 h before treatment. ABs were simultaneously added to the culture medium.

Cell Uptake and Biodistribution

To label nanoparticles, DiI (Invitrogen, USA) was added to nanoparticle solution (1:500) at 37 °C for 30 min. Labelled NP-TPI1 and NP-TPI1/P were administrated into Raw264.7 cells that were seeded in 96-well plates, and incubated for 6 h along with ABs. Images were obtained using the High-Content Cell Cloud Quantification System PE Opera Plenix (PerkinElmer) at 60 min. Labelled NP-TPI1 and NP-TPI1 were intravenously administered to AMI mice at a dose of 200 μg one day after AMI surgery. After 60 min of skin preparation, the fluorescence signal in vivo was detected using an in vivo imaging system (IVIS; PerkinElmer, USA). The major organs including hearts, lungs, livers, kidneys, and spleens, were then harvested to detect fluorescence intensity ex vivo. Afterwards, hearts were sliced into 5-μm sections, stained with DAPI (Beyotime, China), and mounted. The number of DiI nanoparticles per high-power field (HPF) was calculated to further evaluate the cardiac targeting capabilities of NP-TPI1 and NP-TPI1.

Cell Treatment and Evaluations

Raw264.7 cells were seeded and incubated for 24 h, and ABs and one of the following were then added to the culture medium and incubated for another 6 h: PBS, TPI1 (1.25 μg/mL), NP (2.42 μg/mL), NP-TPI1 (3.67 μg/mL) or NP-TPI1/P (3.50 μg/mL).[22] The doses were determined based on the drug-loading rate. The cells were then washed thrice with PBS. For the efferocytosis

experiment, DiD (Invitrogen) was added to the AB solution (1:500) at 37 °C for 30 min. DiD-labelled ABs and one of the treatments (PBS, NP, TPI1, NP-TPI1, NP-TPI1/P) were applied, and images were obtained using the high-content cell cloud quantification system PE Opera Plenix at 60 min and 180 min. For immunofluorescence (IF) staining, the cells were fixed using 4% paraformaldehyde (PFA) for 20 min, and blocked with goat serum (ZSGB-Bio, China). Afterwards, cells were sequentially stained with primary antibodies (Anti-p-SHP1 antibody [ab131500, Abcam, USA] or Anti-CD206 [ab64693, Abcam, USA]), and AF-594-conjugated Goat Anti-Rabbit IgG H&L (ab150080, Abcam, USA), and finally, DAPI (Beyotime, China). Images were obtained using Laser confocal microscope SP8 (Leica, Germany). Total mRNA of Raw264.7 cells was extracted using TRIzol solution and stored at −80 °C. Then, GoScript™ Reverse Transcription kit (Promega, USA) was used to synthesize cDNA. All primer sequences were synthesized by Sangon Biotech (China) according to PrimerBank (https://pga.mgh.harvard.edu/primerbank/) and were. Quantitative PCR was performed using the SYBR Green Real-Time PCR Master Mix (Yeasen, China).

AMI Model Establishment and Treatment

Male C57BL/6J mice, aged eight weeks (wild-type, weighing 18–22 g, Charles River), were randomly assigned to various groups and placed in separate cages. Prior to the surgery, the mice were anesthetized through an intraperitoneal injection of 2% tribromoethanol at a dose of 10 μL/g body weight (Sigma-Aldrich). In the AMI group, the left anterior descending (LAD) coronary artery was ligated. Mice in the sham group underwent an identical surgical procedure, but without the ligation of the LAD.[3] PBS, TPI1 or nanoparticles (NP, NP-TPI1 and NP-TPI1/P, all in 100 μL PBS) were injected via the tail vein on days 1, 2, and 3 post-AMI.[3,15] All mice were provided food and water ad libitum, with 3–4 mice housed per cage. Mice experiencing rapid weight loss or approaching the agonal stage were excluded from the analysis and humanely euthanized. The investigators remained blinded until the completion of the analysis. To minimize potential confounding factors, cage placement and all experimental procedures were randomized. The number of included mice was 5–6 per group for ECG and 9–10 for histological and molecular biological assessments. The determination of sample size was based on previously reported studies.[3,11,12]

To assess cardiac function, transthoracic ECG was performed at days 7 and 21 post-AMI using the VisualSonics Vevo 2100 imaging system (FUJIFILM, Canada). The mice were induced with 3% isoflurane and maintained under anesthesia with 1–1.5% isoflurane in a 95% oxygen mixture. The anesthetic depth was adjusted to achieve a heart rate of 450–550 beats per minute (bpm). Left ventricular (LV) ejection fraction (EF) was assessed using the Parasternal long axis M-mode at the mid-ventricular level. Each parameter was measured three times, and the average values were used for analysis. All mice successfully recovered from anesthesia without any complications.

Histological Analysis

At the end of the study, all mice were euthanized using inhalation anesthesia (5% isoflurane) followed by cervical dislocation for tissue harvesting. The hearts, livers, lungs and kidneys were harvested and fixed in 4% PFA for 18~36 hours, imbedded in paraffin and sliced into 5-μm slides. Hematoxylin and eosin (H&E) staining was performed using HistoCore SPECTRA Workstation (Leica, USA). Sirius red staining using Modified Sirius red stain kit (Solarbio, China) was performed to quantify the fibrosis area (shown as red area) in the left ventricle (LV) with ImageJ software.[3] For IF staining, slides were blocked by 0.3% Triton-X-contained goat serum for 30 min after antigen retrieval. Primary antibodies (Anti-p-SHP1 antibody, Anti-cleaved caspase 3 [9661, Cell signaling, USA], Anti-Mac3 [550292, B&D biosciences, USA] and Anti-CD206). DAPI was used to show the nucleus. All images were obtained using Pannoramic Scanner (3DHISTECH, Hungary).

Enzyme-Linked Immunosorbent Assay (ELISA)

Proteins of hearts harvested at day 3 were extracted using RIPA lysis buffer (Solarbio, China) which contained Phenylmethanesulfonyl fluoride (PMSF, 1Mm, Beyotime, China). The concentrations of interleukin (IL)-1β, tumor necrotic factor (TNF)-α, IL-4, and IL-10 were measured using ELISA kits (Elabscience, China) according to the manufacturer's instructions.

Statistical Analysis

All data are presented as mean ± standard deviation (SD). Statistical analyses were conducted using GraphPad 8.0 (GraphPad Software, USA). To compare two groups, Student's *t*-test was applied, while one-way ANOVA followed by Tukey's test was used for comparisons involving three or more groups. For the in vitro phagocytic assay, two-way ANOVA was utilized. A significance level of $p < 0.05$ was considered for all comparisons. All exact p values were listed in the Supplementary file.

Results

Preparation and Characterization of Nanoparticles in This Study

After acute myocardial ischemia, natural clearance of apoptotic cells in border zone is unsatisfying (Figure 1a), which could be at least partly attributed to a significant upregulation of CD47, a key "don't-eat-me" signal (Figure 1b). Thus, we synthesized a polymer-based nanoparticle (PLGA@PDA, referred to them as NP) to carrying TPI1, an inhibitor of the downstream of CD47 (NP-TPI1; Figure 1c). To further enhance cardiac targeting capability, surface functionalization of NP-TPI1 with cardiac homing peptide (CSTSMLKAC) was conducted (NP-TPI1/P; Figure 1d).

The CHP conjugation was verified using Coomassie brilliant blue staining, where blots of CHP were observed in NP/P (Figure 2a). The mean diameters of NP, NP-TPI1, NP/P, and NP-TPI1/P were 114.2, 118.3, 121.5, and 122.9 nm, respectively (Figure 2b). The ultraviolet absorbance was shown in Figure 2c, and absorption at 247nm was used to calculate the concentration of TPI1 in solution (Figure 2d). The LE and EE of TPI1 in NP-TPI1 were 34.07% and 72.10%, and those in NP-TPI1/P were 35.69% and 69.24%, respectively. Additionally, the NP, NP-TPI1 and NP-TPI1/P share similar two-layer spherical shape (Figure 2e). The mean potentials of NP, NP-TPI1, NP/P, NP-TPI1/P are −12.1, −9.8, −15.4, −11.9 mV, respectively (Figure 2f). Given the inherent ROS/pH dual responsiveness of PLGA@PDA nanoparticles, the release of the payload of NP-TPI1 and NP-TPI1/P under low pH and hydrogen peroxide were evaluated. Both types of nanoparticles could maintain stability for up to 168 hours at pH 7.4 (with approximately 80% of the particles remaining stable at 168 hours); however, under conditions of low pH (6.8) and H_2O_2, TPI1 release was significantly accelerated, indicating that both nanoparticles could release the drug in AMI lesions which are characterized with evoked production of ROS and low pH (Figure 2g). These findings demonstrated that NP-TPI1 and NP-TPI1/P served as two promising TPI1 nanocarriers.

Pro-Efferocytic and Anti-Inflammatory Effects of NP-TPI1 and NP-TPI1/P in vitro

The pro-efferocytic effects of NP-TPI1 and NP-TPI1/P were examined using Raw264.7 cells. Both nanoparticles could be taken efficiently (Figure 3a). Following TPI1 or different nanoparticles, STS-induced apoptotic bodies were given to Raw264.7 cells; then, the expression level of p-SHP1 were evaluated, which were significantly downregulated in cells treated with either TPI1, NP-TPI1 or NP-TPI1/P (Figure 3b and c). DiO-labelled apoptotic bodies were utilized to analyze the phagocytic efficiency under different interventions. TPI1, NP-TPI1 and NP-TPI1/P exerted similar pro-efferocytic effects at 60 min; while the nanoparticles carrying TPI1 had a significant higher phagocytic ratio at 180 min, which may be attributed to improved stability in the culture medium (Figure 3d and e). However, no significant differences were observed between the NP-TPI1 and NP-TPI1/P-treated cells.

Given that pro-repair and anti-inflammatory polarization (M2) is induced by the efferocytosis process, the levels of secondary inflammation were assessed. TPI1, NP-TPI1 and NP-TPI1/P significantly promote M2 polarization compared with the PBS and NP groups in terms of the marker, CD206 (Figure 4a and b). However, the effects are comparable among the three groups. The regulation was further verified by the expression levels of inflammation-related markers, including *Il1b, Tnfa, Il10* and *Cd206*. It's important to note that peptide modification did not further enhance the capability of regulating inflammation since no significant differences were observed in either factor between the NP-TPI1 and NP-TPI1/P group (Figure 4c–f). These data indicate that both NP-TPI1 and NP-TPI1/P exert pro-efferocytic and anti-inflammatory effects in vitro. Encapsulation in NP promotes the stability of TPI1 and extend the duration.

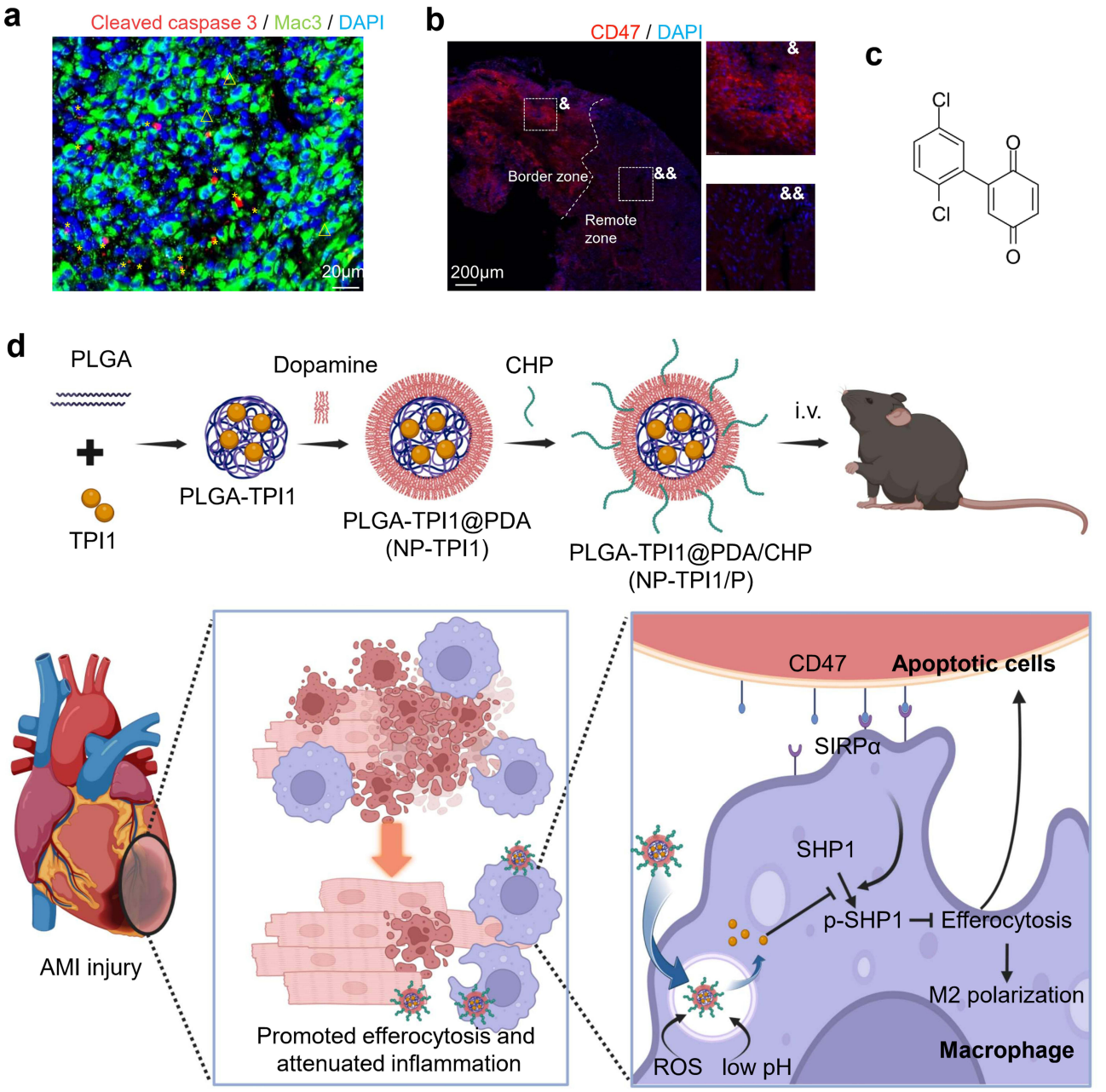

Figure 1 Scheme of cardiac homing peptide-functionalized, TPI-1-loaded PLGA@PDA nanoparticles. (**a**) Delayed clearance of apoptotic cells in border zone. Bar=20μm. (**b**) Upregulation of CD47 in the border zone (and) compared with remote zone (andand). Bar=200μm. (**c**) The structure of TPI1. (**d**) Scheme of the study. Construction of TPI1-loaded PLGA@PDA nanoparticles (NP-TPI1) and cardiac homing peptide (CHP)-modified NP-TPI1 (NP-TPI1/P) is shown. The NP-TPI1/P is designed to release the payload under ROS and low pH in AMI lesion and TPI1 inhibits the phosphorylation of SHP1, canceling the impairment of efferocytosis.
Abbreviations: PLGA@PDA, poly (lactic-co-glycolic acid) @polydopamine. CHP, cardiac homing peptides. i.v., injected intravenously. SIRPα, Signal regulatory protein α. SHP1, Src homology 2 domain-containing phosphatase-1. AMI, acute myocardial infarction.

The Pro-Efferocytic and Anti-Inflammatory Effects of NP-TPI1 and NP-TPI1/P in AMI Mice

The cardiac targeting capability of NP-TPI1 and NP-TPI1/P were assessed. Fluorescent signal was only observed in mice received NP-TPI1/P administration, while the signals of NP or NP-TPI1 in hearts were not strong enough to be detected (Figure 5a and b). Further investigations on cardiac sections proved the improved retention of the CHP-decorated nanoparticles in border zone (Figure 5c and d).

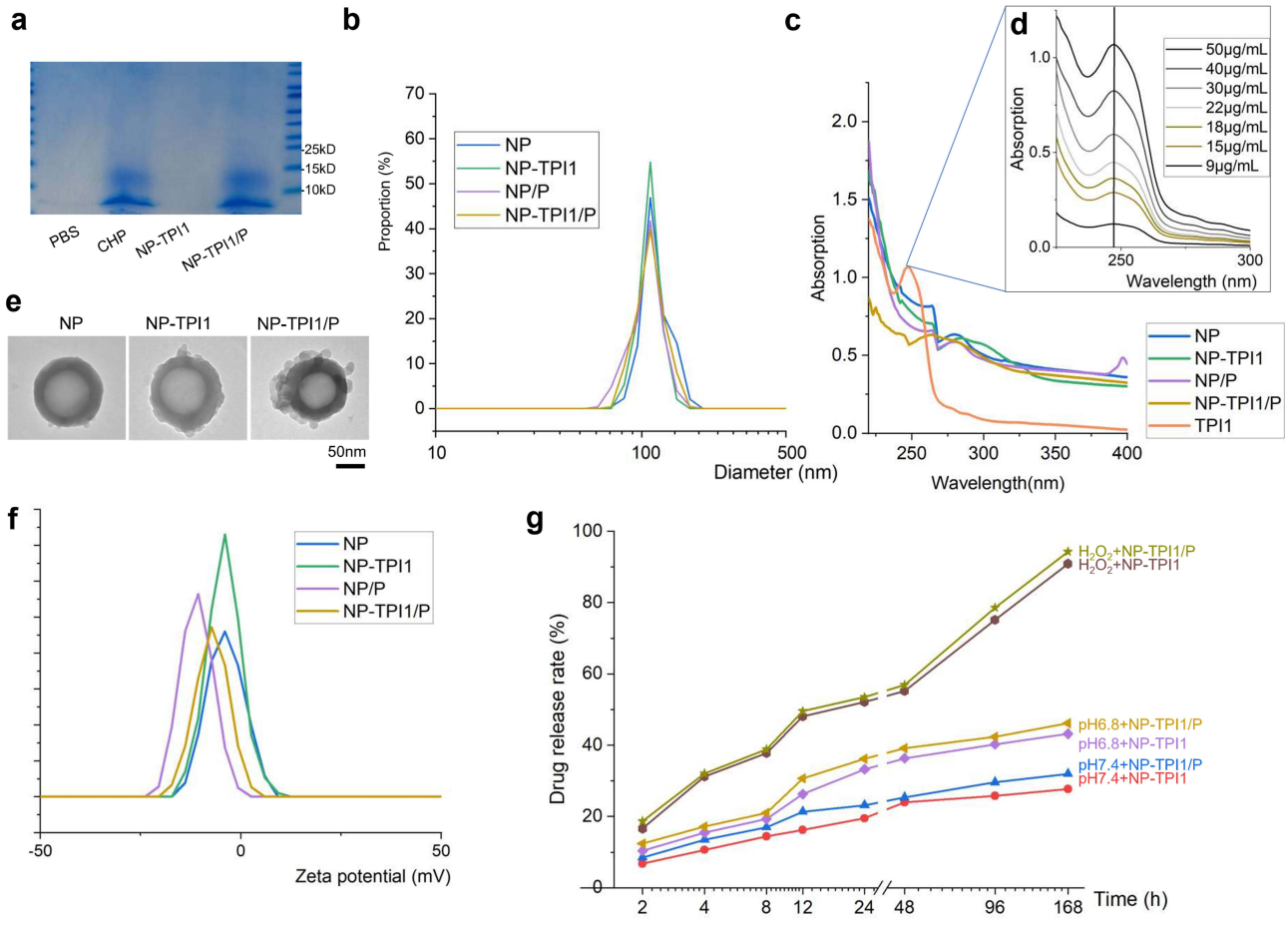

Figure 2 The characterization of nanoparticles in this study. (**a**) The Coomassie Brilliant Blue staining results revealing the conjugation of CHP on NP-TPI1. (**b**) The size distribution of NP (PLGA@PDA), NP-TPI1, NP/P, and NP-TPI1/P in this study. (**c**) The ultraviolet absorption of TPI1, NP, NP-TPI1, NP/P, and NP-TPI1/P. (**d**) The absorption at 247nm was used to assess the concentration of TPI1 in solution. (**e**) Representative Transmission Electron Microscopy (TEM) images of NP, NP-TPI1 and NP-TPI1/P. Bar=50nm. (**f**) The zeta potential of NP, NP-TPI1, NP/P, and NP-TPI1/P in this study. (**g**) The drug release curve of NP-TPI1 and NP-TPI1/P under different conditions. Low pH (6.8) and hydrogen peroxide enhanced the release of TPI1.

To assess the pro-efferocytic and anti-inflammatory effects of NP-TPI1 and NP-TPI1/P in vivo, an AMI mice model was applied. Hearts were harvested 12 hours after the final dose of intravenous administration (Figure 5e). The phosphorylation levels of SHP1 were decreased in the two groups (Figure 5f and g); consistently, a significant improvement of phagocytic efficiency was observed in the NP-TPI1 and NP-TPI1 groups (Figure 5h and i). Importantly, the peptide modification further enhanced both effects. The evoked inflammation was also attenuated by the two TPI1-loaded nanoparticles, as demonstrated in H&E and CD206 IF staining (Figure 6a–c), and levels of inflammatory factors in hearts (Figure 6d–g). These data indicate that NP-TPI1 and NP-TPI1/P emerge as novel candidates for promotion of efferocytosis and regulation of inflammation, wherein NP-TPI1/P exhibits a particularly pronounced efficacy.

The Long-Term Cardioprotective Effects of NP-TPI1 and NP-TPI1/P in AMI Mice

To assess the long-term effects of NP-TPI1 and NP-TPI1/P on cardiac performance and remodeling, tissues were harvested 21 days after infarction (21dpi; Figure 7a). The LVEF was significantly improved in the NP-TPI1/P group at 7dpi; while both NP-TPI1 and NP-TPI1/P improved cardiac function at 21dpi compared with the PBS, NP and TP1 groups (Figure 7c and d). Administration of TPI1 enabled a moderated improvement in LVEF at 21dpi. Histological evaluation revealed a significant attenuation of fibrosis, the characteristic change in post-AMI remodeling, in TPI1, NP-TPI1 and NP-TPI1/P-treated mice, with the most pronounced effect observed in the NP-TPI1/P group (Figure 7e and f).

https://doi.org/10.2147/IJN.S533628

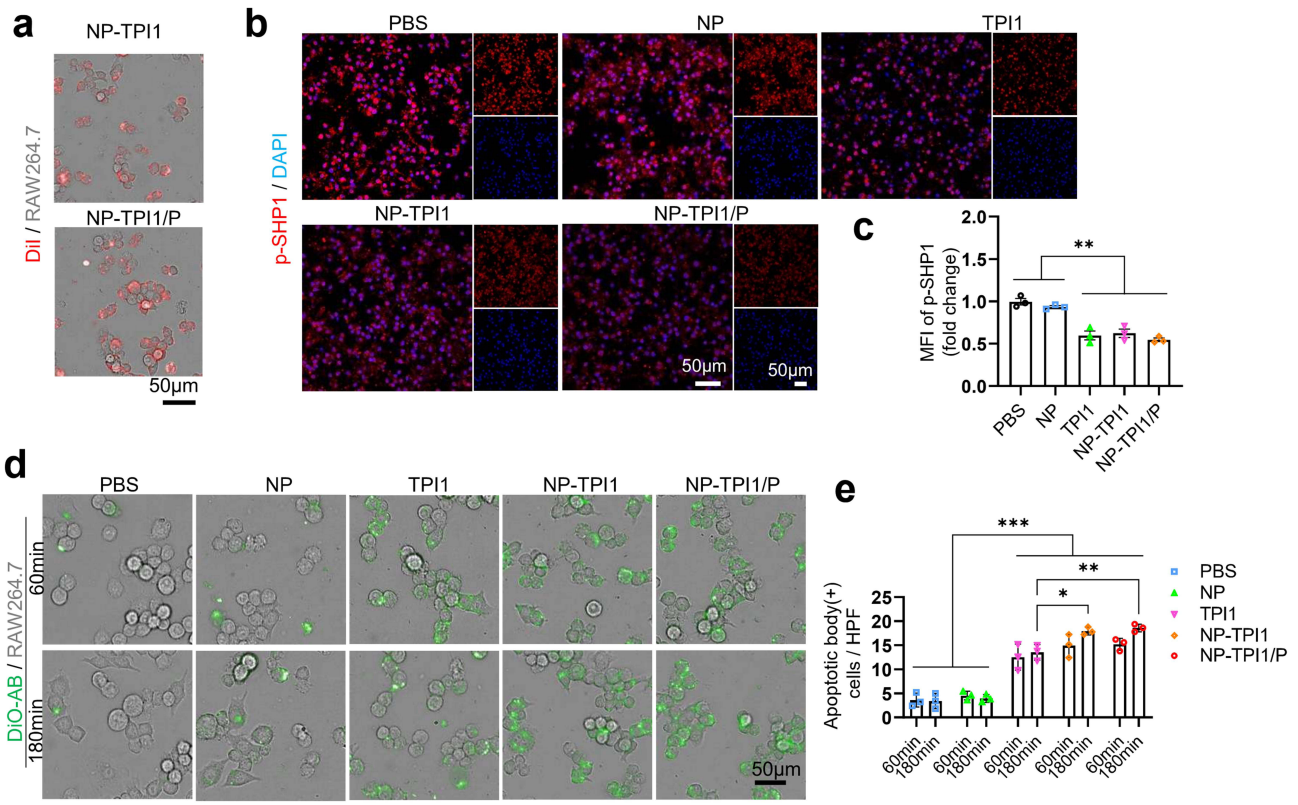

Figure 3 Inhibition of phosphorylation of SHP1 and promotion of efferocytosis in RAW264.7 cells treated with nanoparticles in vitro. (**a**) Cellular uptake of NP-TPI1 and NP-TPI1/P. Bar=50μm. (**b** and **c**) The representative images (**b**) and quantitative analysis (**c**) of p-SHP1 in Raw264.7 cells, indicating that either TPI1, NP-TPI1 or NP-TPI1/P could inhibit the phosphorylation of SHP1. Experiments were conducted in the presence of apoptotic bodies. MFI, mean fluorescence intensity. Bar=50μm. (**d** and **e**) The representative images and quantitative analysis of engulfed DiO-labelled apoptotic bodies (ABs) in Raw264.7 cells under different treatments, indicating that TPI1 encapsulated in nanoparticles exhibited a more sustained phagocytosis-promoting effect compared to free TPI1. HPF, high power field. Bar=50μm. Statistical analysis was performed using One-way (**c**) or Two-way (**e**) ANOVA. *p<0.05, **p<0.01, ***p<0.001.

Given the crucial role of the CD47/SIRPα/SHP1 signaling pathway and the associated M2 polarization in macrophage recognition of autologous cells, regulation of tissue fibrosis, and maintenance of normal immune function, it is imperative to investigate the biocompatibility of these processes. No significant abnormality was observed in the lung, kidney and liver in all groups. Besides, no significant liver fibrosis was found (Figure 7g). These results showed that both NP-TPI1 and NP-TPI1/P are two promising tools to protect hearts against AMI with no obvious toxicity.

Discussion

In this study, we engineered a novel PLGA@PDA nanoparticle encapsulating TPI1 (NP-TPI1) and demonstrated its potent efficacy in facilitating phagocytosis and modulating polarization both in vitro and in an AMI mouse model. Modification with CHP (NP-TPI1/P) further augmented its cardiac targeting capability, while preserving its intrinsic protective effects, thereby significantly enhancing its protective action in vivo. This study presents an innovative, dual-purpose nanotherapeutic strategy grounded in efferocytosis following myocardial infarction, providing a novel intervention with the potential to enhance post-infarction cardiac function and mitigate the worldwide health toll associated with myocardial infarction.

Recently, the development of nanomaterials for targeted drug delivery, including polymeric, metal, and lipid nanoparticles, has provided attractive therapeutic options for cardiovascular diseases. Among them, polymeric nanoparticles such as PLGA nanoparticles are of great interest owing to their biocompatibility, stability, ease of production, and Food and Drug Administration (FDA) approval.[23,24] PDA modification can enhance stability and act as a ROS scavengers.[10,25] In an infarcted niche where ROS and low pH are characteristic, PLGA@PDA NP significantly released the payload, as shown in our study and in a series of previous reports.[17,26,27] This may explain why NP-TPI1(/P)

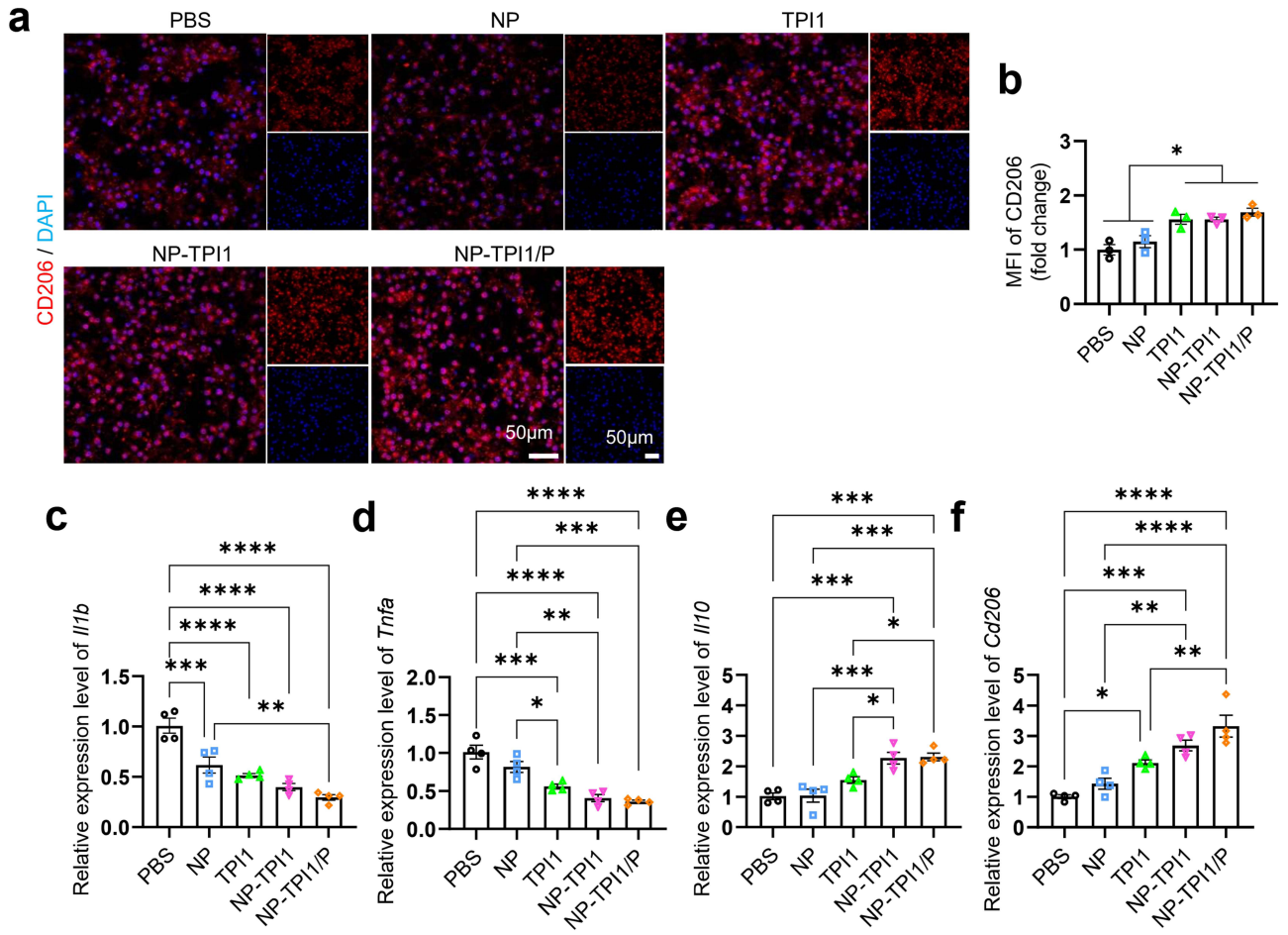

Figure 4 Inhibition of inflammation and the promotion of M2 polarization in Raw264.7 cells treated with nanoparticles in vitro. (**a** and **b**) The representative images of CD206 staining (**a**) and quantitative analysis (**b**) in Raw264.7 cells, indicating that either TPI1, NP-TPI1 or NP-TPI1/P could promote the M2 polarization. Experiments were conducted in the presence of apoptotic bodies. Bar=50μm. (**c–f**) The relative expression levels of *Il1b, Tnfa, Il10* and *Cd206* mRNA, as measured by real-time qPCR. *Il1b* and *Tnfa* are markers of pro-inflammatory M1 macrophage markers, while *Il10* and *Cd206* are markers of anti-inflammatory, pro-repair M2 macrophage markers. Experiments were conducted in the presence of apoptotic bodies. *Il1b*, interleukin 1β. *Tnfa*, tumor necrotic factor α. *Il10*, interleukin 10. Statistical analysis was performed using One-way ANOVA. **p*<0.05, ***p*<0.01, ****p*<0.001, *****p*<0.0001.

accumulated in the liver, but failed to induce hepatotoxicity. An in vitro study showed that the two TPI1-loaded NPs had similar levels of phagocytosis promotion and macrophage polarization regulation with TPI1 at the same dose at 60 min. However, NP encapsulation improved at 180 min, which revealed higher stability in the culture medium, extended efficient duration, or controlled release. However, even with ROS/low pH responsiveness, these particles still lack active targeting to injured myocardium. Several engineering strategies have been preliminarily explored, such as fusion or coating with the cell membranes of macrophages and platelets[3,15,28] and decoration with targeting molecules (including ligands, homing peptides, and monoclonal antibodies).[29–31] For example, Li et al used neutrophil membrane-coated allicin-loaded silica nanoparticles for the treatment of myocardial infarction.[12] The targeting capability was achieved through the interaction between β2 integrin and intercellular adhesion molecule-1 (ICAM-1) on the surface of endothelial cells. Similarly, macrophage membranes mimicking the recruitment and chemotaxis process to the inflammatory lesions, and platelet membranes recognizing damaged endothelium via glycoproteins, are also widely used for nanoparticle modification.[3,11,15] Herein, CHP (CSTSMLKAC) rather than antibody decoration or membrane coating was chosen because of its lower cost, higher safety, and smaller batch differences, which are essential for clinical translation.[13,15,31] CHP-conjugated nanoparticles have been used in several pilot studies. For instance, CHP-conjugated exosomes increase the delivery of cardioprotective extracellular nanovesicles to infarcted hearts, reduce fibrosis, and promote cellular proliferation and angiogenesis.[29] Genetically engineered CHP-expressing exosomes developed by Wang et al exerted

https://doi.org/10.2147/IJN.S533628

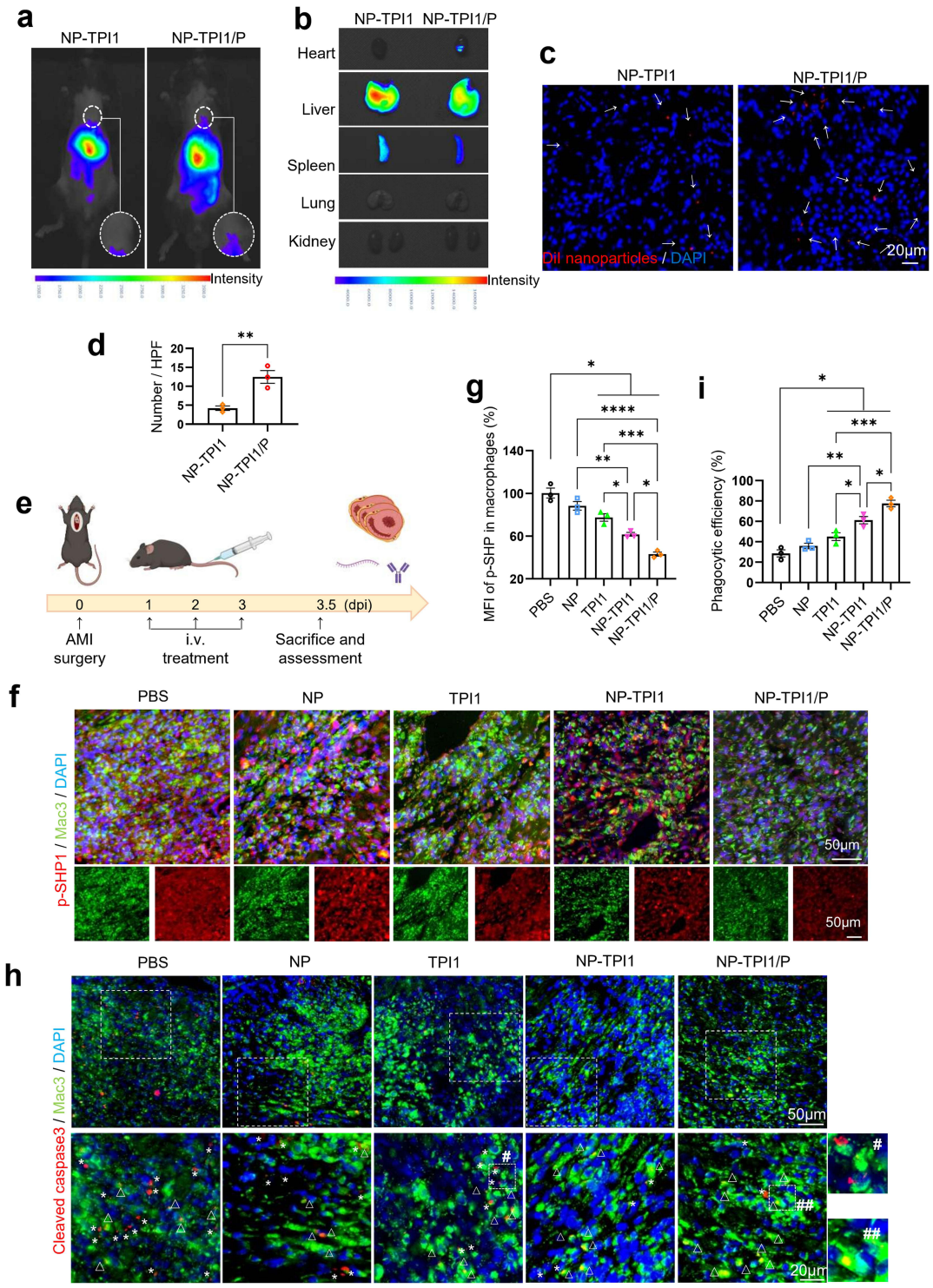

Figure 5 The NP-TPI1/P enhanced cardiac homing capability and promoted the efferocytosis. (**a**) The in vivo imaging results of AMI mice 1 hour after injected with DiI-labelled NP-TPI1 and NP-TPI1/P. (**b**) The ex vivo imaging results of AMI mice 1 hour after injected with DiI-labelled NP-TPI1 and NP-TPI1/P. (**c** and **d**) The representative images (**c**) and quantitative analysis (**d**) of nanoparticles in AMI area, suggesting a higher level of lesional retention of NP-TPI1/P. DiI-labelled nanoparticles were shown as red puncta (arrows). Bar=20μm. (**e**) Animal experiment scheme for acute effects of SHP1 phosphorylation and efferocytosis of nanoparticles. (**f** and **g**) The representative images (**f**) and the quantitative analysis (**g**) of macrophage p-SHP1 expression, indicating that NP-TPI1/P treatment led to the most pronounced inhibition of macrophage p-SHP1 in AMI lesions. Macrophages were shown as Mac-3 (Green). Bar=50μm. (**h** and **i**) The representative images (**h**) and the quantitative analysis (**i**) of apoptotic bodies (AB) in AMI lesions, showing that NP-TPI1/P treatment led to the most pronounced promotion of efferocytosis. Apoptotic bodies were shown as cleaved caspase 3 puncta (red), and the phagocytic efficiency was calculated as (number of AB that were not been engulfed by macrophages shown as "*")/(number of total AB). Those AB engulfed by macrophages were shown as "Δ". Examples of AB that was not engulfed, and engulfed by macrophages were shown in the right (# and ##, respectively). Bar=50μm or 20μm. Statistical analysis was performed using Student's *t* test (**d**) or One-way ANOVA. **p*<0.05, ***p*<0.01, ****p*<0.001, *****p*<0.0001.

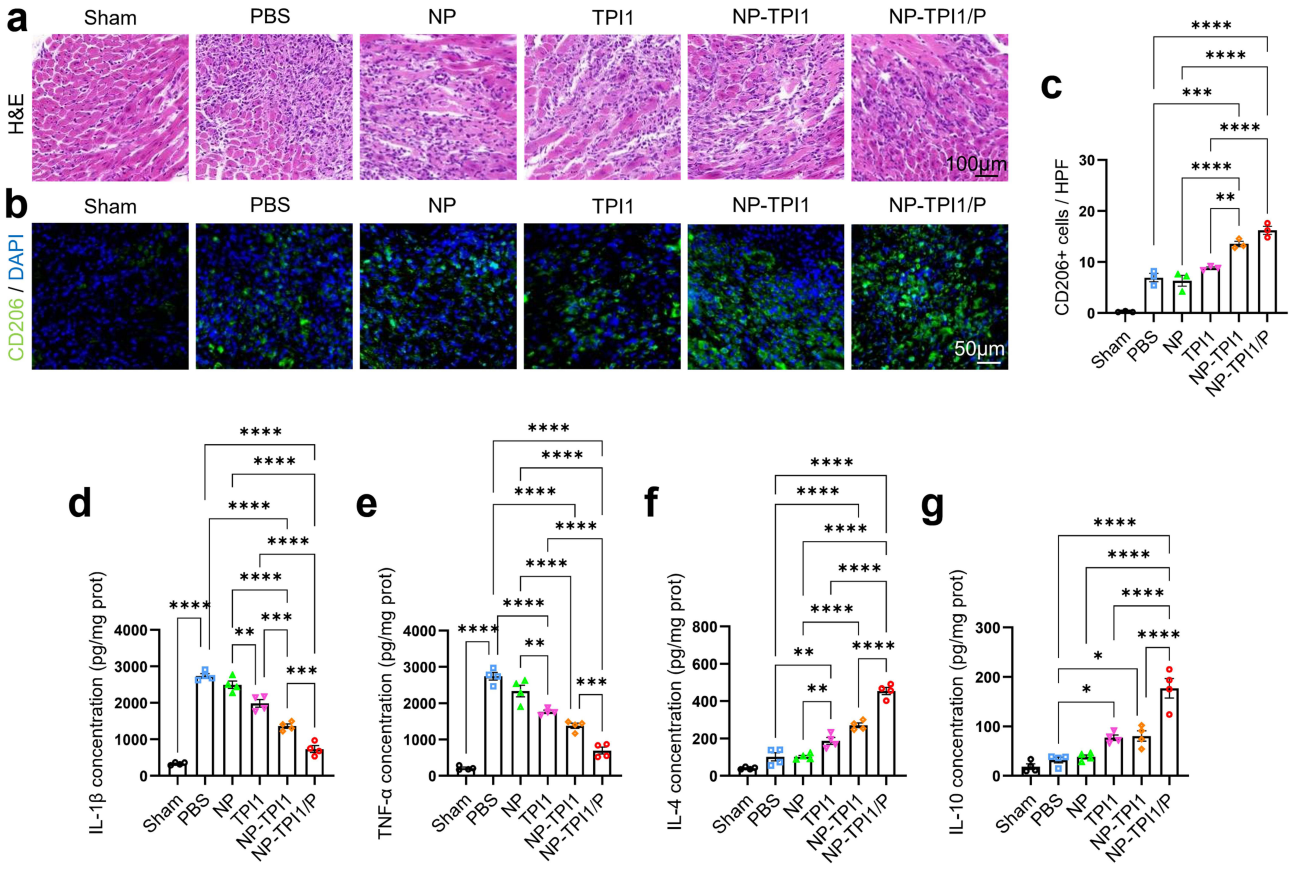

Figure 6 Inhibition of secondary inflammation in AMI mice treated with NP-TPI1 and NP-TPI1/P. (**a** and **b**) The representative images of H&E staining (**a**) and CD206 immunofluorescence staining (**b**), showing that mice administrated with NP-TPI1/P had the highest level of anti-inflammatory and pro-repair M2 polarization in AMI lesions. Bar= 100μm and 50μm, respectively. (**c**) The quantitative analysis of CD206 positive cells in border zone. (**d**–**g**) The ELISA results of pro-inflammatory factors ((**d**), IL-1β; (**e**), TNF-α) and anti-inflammatory factors ((**f**), IL-4; (**g**), IL-10). Statistical analysis was performed using One-way ANOVA. *p<0.05, **p<0.01, ***p<0.001, ****p<0.0001.

a similar function.[30] Sun et al constructed a CHP-triphenylphosphonium cation conjugate to effectively promote intravenous mitochondrial transplantation into the ischemic lesion.[14] It is interesting to note that the signal of TPI1-loaded NP without CHP modification was too weak to be detected in the heart, while moderate cardioprotective effects were observed, indicating a relatively small number of nanoparticles reaching lesions, or the payload may be released by those accumulated in other tissues and delivered to heart via blood.

Dead cells and cell debris can become secondarily necrotic and evoke inflammatory reactions, which can lead to the deterioration of cardiac function and remodeling;[3,32] while some apoptotic cell components could serve as signaling molecules and metabolites for metabolic reprogramming, and contribute to M2 polarization.[32,33] Thus, efferocytosis limits necrosis and also contributes to the pro-resolving and pro-repairing signaling in macrophages via the cargo released from apoptotic cells after engulfment and phagolysosomal digestion. Due to a series of disorders of the "eat-me" and "don't'-eat-me" signals, efferocytosis is impaired under various pathologic conditions including myocardial ischemia and accordingly, clearance of dead cell has been recognized as a novel therapeutic target.[34,35] For instance, Chuang et al developed a chimeric antigen receptor (CAR) macrophage targeting CD47 on the surface of apoptotic cells to withstand the immunosuppressive inflammatory environment.[36] In some pilot studies, several targeted nanoparticles that promote efferocytosis have been developed, and no significant side effects (eg, anemia) were observed.[37] Song et al engineered platelet membrane-coated hollow mesoporous silicon nanoparticles to deliver a ferroptosis inhibitor and an anti-CD47 antibody to promote phagocytosis.[11] CpG, a Toll-like receptor 9 agonist, has been identified as an activator of macrophage efferocytosis in atherosclerosis therapy.[38] Tang et al developed CpG-conjugated AgNPs to enhance efferocytosis and regulate inflammation by inducing a metabolic shift in the macrophages. Additionally, a dexamethasone-loaded glycyrrhiza protein-based nanoparticle was developed to induce apoptosis of neutrophils, which were further engulfed by macrophages, thus promoting their polarization into an anti-inflammatory state (M2). The

https://doi.org/10.2147/IJN.S533628

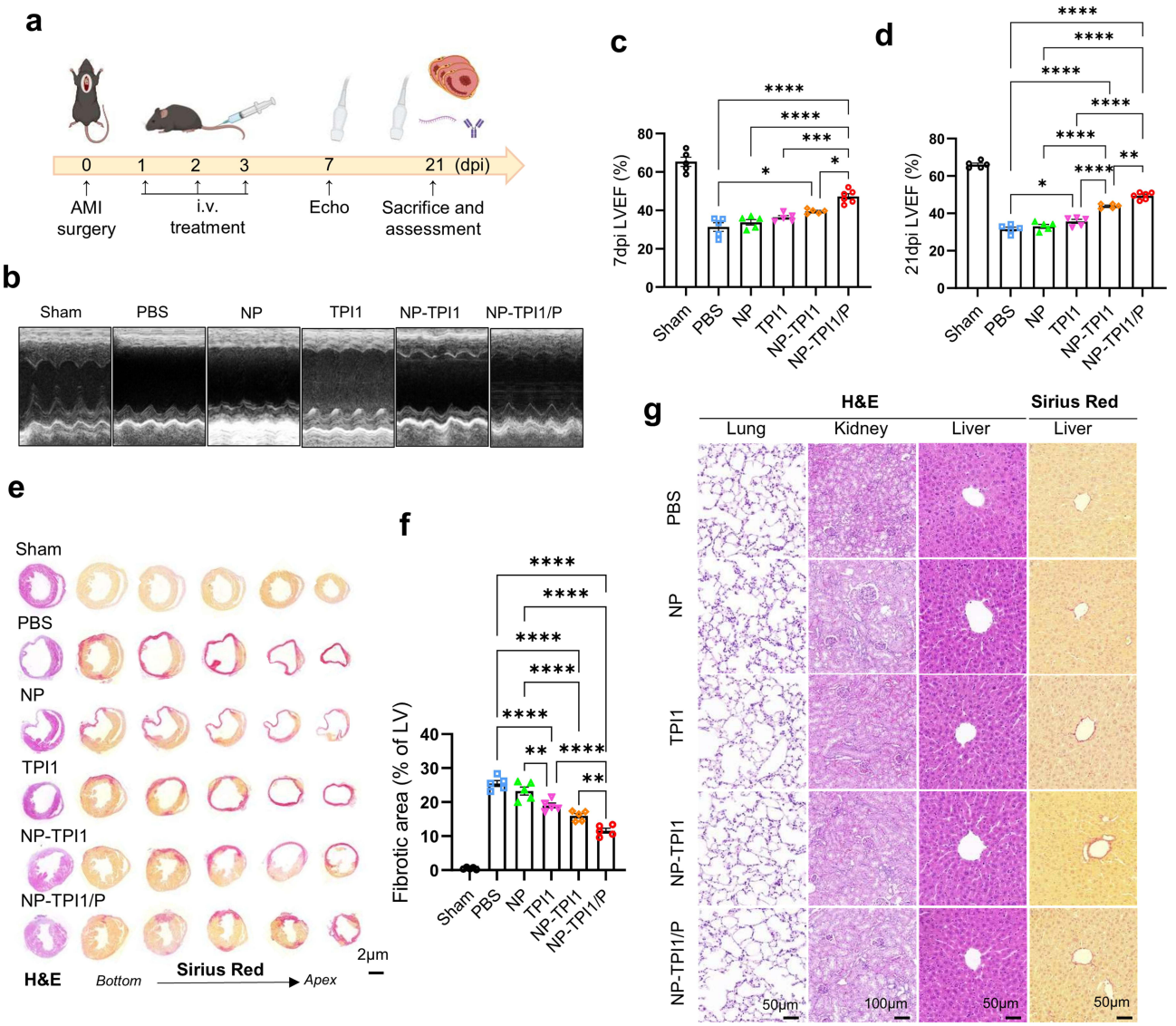

Figure 7 The long-term cardioprotective effects of NP-TPI1 and NP-TPI1/P. (**a**) The study scheme for the long-term cardioprotective effects of different treatment. (**b**) The representative images of echocardiography 21 days after infarction (21dpi). (**c** and **d**) The analysis of left ventricular ejection fraction (LVEF) 7dpi and 21dpi, indicating that mice treated with NP-TPI1/P had the most significant improvement in cardiac function compared to the PBS group. (**e** and **f**) The representative images and quantitative analysis of H&E and Sirius Red staining, showing that mice treated with NP-TPI1/P had the smallest fibrotic area post-AMI. The fibrotic area was shown as the red area in the multi-layered Sirius red staining. Bar=50μm. (**g**) The representative H&E and Sirius Red staining images of major organs. Bar=50, 100, 50 and 50μm, respectively. Statistical analysis was performed using One-way ANOVA. **p*<0.05, ***p*<0.01, ****p*<0.001, *****p*<0.0001.

delivery of the nanoparticle into macrophages also enabled dexamethasone to further modulate macrophage function.[39] In a marvelous study, a hybridized nanoparticle using red blood cell (RBC) membrane that highly expresses CD47 and is conjugated to Ly6G antibody targeting neutrophils.[40] The senescent RBC-mimetic liposomes were able to accumulate in the infarcted myocardial tissue, where they inhibited the CD47-SIRPα interaction, and thus, facilitated the efferocytosis of apoptotic cardiomyocytes and enhanced heart repair. Similarly, Lai et al have developed a triple-membrane fused hybrid particle that exhibits anti-apoptotic, anti-inflammatory, and efferocytosis-promoting properties.[3] TPI1-loaded liposomes coated with macrophage membrane were also prepared by Sha et al and the pro-efferocytic function was evaluated in atherosclerotic mice,[15] where the phosphorylation of SHP1 was significantly blocked and the efferocytosis was reversed. In the present study, we put forward a novel dual-responsive, myocardium-targeting nanoparticle for AMI treatment which simultaneously facilitated clearance of apoptotic cells and mitigated inflammation, thereby providing a synergistic protective effect on the heart. Besides, the current

nanoplatform is considered more amenable to large-scale production, as they are not constrained by the limitations associated with cell membrane extraction.[10]

One limitation of this study is that it does not provide mechanistic insights linking efferocytosis restoration and inflammation alleviation. This is due to the fact that, as indicated by previously reports, pathways involving Signal Transducer and Activator of Transcription 6 (STAT6), Sirtuin1, Vascular endothelial growth factor C, lactate, and tryptophan metabolism are all involved.[5,41–43] Further mechanistic studies on TPI1-NP/P or other nanoparticles targeting efferocytosis are warranted. Another limitation is that female mice were not included in the current study. This is to enhance the reliability and reproducibility of the results, as female individuals exhibit resistance to myocardial ischemia due to hormonal influences and certain pathways.[1,44]

Conclusively, we fabricated a cardiac-targeting bifunctional nanoparticles based on SHP1 inhibitor (NP-TPI1) with excellent safety. By blocking the downstream of CD47/SIRPα signal, the impaired removal of dead cells and extended inflammation were reversed. Specific peptide modification enhanced cardiac targeting capability without influencing the inherent benefits, thus further improving the efficacy in vivo. Collectively, this study provided a novel, promising strategy for AMI based on an essential mechanism recognized recently, with significant potential for clinical translation.

Data Sharing Statement

All data generated or analyzed during this study are included in this published article.

Ethics Approval and Informed Consent

The study was approved by The Animal Care and Use Committee of Fuwai Hospital, Peking Union Medical College of Medicine (FW-2023-0026). All institutional and national guidelines for the care and use of laboratory animals were followed.

Funding

The work was supported by National Natural Science Foundation of China (ID: 82100313). The sponsor(s) were not involved in the design or process of the project.

Disclosure

The authors report no conflicts of interest in this work.

References

1. Collaborators GCoD. Global, regional, and national age-sex-specific mortality for 282 causes of death in 195 countries and territories, 1980-2017: a systematic analysis for the global burden of disease study 2017. *Lancet*. 2018;392(10159):1736–1788. doi:10.1016/s0140-6736(18)32203-7
2. Zhang W, Zhao J, Wang R, et al. Macrophages reprogram after ischemic stroke and promote efferocytosis and inflammation resolution in the mouse brain. *CNS Neurosci Ther*. 2019;25(12):1329–1342. doi:10.1111/cns.13256
3. Lai J, Pan Q, Chen G, et al. Triple hybrid cellular nanovesicles promote cardiac repair after ischemic reperfusion. *ACS Nano*. 2024;18 (5):4443–4455. doi:10.1021/acsnano.3c10784
4. Wan E, Yeap XY, Dehn S, et al. Enhanced efferocytosis of apoptotic cardiomyocytes through myeloid-epithelial-reproductive tyrosine kinase links acute inflammation resolution to cardiac repair after infarction. *Circ Res*. 2013;113(8):1004–1012. doi:10.1161/circresaha.113.301198
5. Glinton KE, Ma W, Lantz C, et al. Macrophage-produced VEGFC is induced by efferocytosis to ameliorate cardiac injury and inflammation. *J Clin Invest*. 2022;132(9). doi:10.1172/jci140685
6. Zhang S, Yeap XY, DeBerge M, et al. Acute CD47 blockade during ischemic myocardial reperfusion enhances phagocytosis-associated cardiac repair. *JACC Basic Transl Sci*. 2017;2(4):386–397. doi:10.1016/j.jacbts.2017.03.013
7. Kojima Y, Volkmer JP, McKenna K, et al. CD47-blocking antibodies restore phagocytosis and prevent atherosclerosis. *Nature*. 2016;536 (7614):86–90. doi:10.1038/nature18935
8. Poon IK, Lucas CD, Rossi AG, Ravichandran KS. Apoptotic cell clearance: basic biology and therapeutic potential. *Nat Rev Immunol*. 2014;14 (3):166–180. doi:10.1038/nri3607
9. Henson PM, Tuder RM. Apoptosis in the lung: induction, clearance and detection. *Am J Physiol Lung Cell Mol Physiol*. 2008;294(4):L601–11. doi:10.1152/ajplung.00320.2007
10. Pan Q, Xu J, Wen CJ, Xiong YY, Gong ZT, Yang YJ. Nanoparticles: promising tools for the treatment and prevention of myocardial infarction. *Int J Nanomed*. 2021;16:6719–6747. doi:10.2147/ijn.S328723
11. Song L, Yuan X, Zhao Z, Wang P, Wu W, Wang J. A biomimetic nanocarrier strategy targets ferroptosis and efferocytosis during myocardial infarction. *Int J Nanomed*. 2024;19:8253–8270. doi:10.2147/ijn.S461212

12. Li M, Wu J, Yang T, et al. Engineered biomimetic nanoparticles-mediated targeting delivery of allicin against myocardial ischemia-reperfusion injury by inhibiting ferroptosis. *Int J Nanomed*. 2024;19:11275–11292. doi:10.2147/ijn.S478276
13. Ma C, Yang Z, Wang J, et al. Exosomes miRNA-499a-5p targeted CD38 to alleviate anthraquinone induced cardiotoxicity: experimental research. *Int J Surg*. 2024;110(4):1992–2006. doi:10.1097/js9.0000000000001118
14. Sun X, Chen H, Gao R, et al. Intravenous transplantation of an ischemic-specific peptide-TPP-mitochondrial compound alleviates myocardial ischemic reperfusion injury. *ACS Nano*. 2023;17(2):896–909. doi:10.1021/acsnano.2c05286
15. Sha X, Dai Y, Chong L, et al. Pro-efferocytic macrophage membrane biomimetic nanoparticles for the synergistic treatment of atherosclerosis via competition effect. *J Nanobiotechnol*. 2022;20(1):506. doi:10.1186/s12951-022-01720-2
16. Zong L, Wang Q, Sun H, et al. Intra-articular injection of PLGA/polydopamine core-shell nanoparticle attenuates osteoarthritis progression. *ACS Appl Mater Interfaces*. 2024;16(17):21450–21462. doi:10.1021/acsami.3c18464
17. Nie J, Cheng W, Peng Y, et al. Co-delivery of docetaxel and bortezomib based on a targeting nanoplatform for enhancing cancer chemotherapy effects. *Drug Deliv*. 2017;24(1):1124–1138. doi:10.1080/10717544.2017.1362677
18. Zhang F, Yang Q, Tang S, et al. CD38-targeted and erythrocyte membrane camouflaged nanodrug delivery system for photothermal and chemotherapy in multiple myeloma. *Int J Pharm*. 2023;643:123241. doi:10.1016/j.ijpharm.2023.123241
19. Zhang L, Xiao S, Kang X, et al. Metabolic conversion and removal of manganese ferrite nanoparticles in RAW264.7 cells and induced alteration of metal transporter gene expression. *Int J Nanomed*. 2021;16:1709–1724. doi:10.2147/ijn.S289707
20. Wang Y, Liu B, Lu H, et al. SETD4-mediated KU70 methylation suppresses apoptosis. *Cell Rep*. 2022;39(6):110794. doi:10.1016/j.celrep.2022.110794
21. Qiu S, Liu J, Chen J, et al. Targeted delivery of MerTK protein via cell membrane engineered nanoparticle enhances efferocytosis and attenuates atherosclerosis in diabetic ApoE(-/-) mice. *J Nanobiotechnol*. 2024;22(1):178. doi:10.1186/s12951-024-02463-y
22. Teng R, Wang Y, Lv N, et al. Hypoxia impairs NK cell cytotoxicity through SHP-1-mediated attenuation of STAT3 and ERK signaling pathways. *J Immunol Res*. 2020;2020:4598476. doi:10.1155/2020/4598476
23. Malek-Khatabi A, Sadat Razavi M, Abdollahi A, et al. Recent progress in PLGA-based microneedle-mediated transdermal drug and vaccine delivery. *Biomater Sci*. 2023;11(16):5390–5409. doi:10.1039/d3bm00795b
24. Park JE, Kim WC, Kim SK, et al. Protection of hearing loss in ototoxic mouse model through SPIONs and dexamethasone-loaded PLGA nanoparticle delivery by magnetic attraction. *Int J Nanomed*. 2022;17:6317–6334. doi:10.2147/ijn.S380810
25. Bao X, Zhao J, Sun J, Hu M, Yang X. Polydopamine nanoparticles as efficient scavengers for reactive oxygen species in periodontal disease. *ACS Nano*. 2018;12(9):8882–8892. doi:10.1021/acsnano.8b04022
26. Gupta A, Niveria K, Chandpa HH, et al. Stimuli-responsive magnetic silica-poly-lactic-co-glycolic acid hybrid nanoparticles for targeted cancer chemo-immunotherapy. *Drug Deliv Transl Res*. 2024;14(10):2712–2726. doi:10.1007/s13346-024-01521-0
27. Chen S, Zhou X, Wang X, Li H, An R, Qian Y. Magnetical scafford with ROS-scavenging for bone regeneration under static magnetic field. *Colloids Surf B Biointerfaces*. 2024;245:114245. doi:10.1016/j.colsurfb.2024.114245
28. Li Q, Huang Z, Wang Q, et al. Targeted immunomodulation therapy for cardiac repair by platelet membrane engineering extracellular vesicles via hitching peripheral monocytes. *Biomaterials*. 2022;284:121529. doi:10.1016/j.biomaterials.2022.121529
29. Vandergriff A, Huang K, Shen D, et al. Targeting regenerative exosomes to myocardial infarction using cardiac homing peptide. *Theranostics*. 2018;8(7):1869–1878. doi:10.7150/thno.20524
30. Wang X, Chen Y, Zhao Z, et al. Engineered exosomes with ischemic myocardium-targeting peptide for targeted therapy in myocardial infarction. *J Am Heart Assoc*. 2018;7(15):e008737. doi:10.1161/jaha.118.008737
31. Liu S, Chen X, Bao L, et al. Treatment of infarcted heart tissue via the capture and local delivery of circulating exosomes through antibody-conjugated magnetic nanoparticles. *Nat Biomed Eng*. 2020;4(11):1063–1075. doi:10.1038/s41551-020-00637-1
32. Mehrotra P, Ravichandran KS. Drugging the efferocytosis process: concepts and opportunities. *Nat Rev Drug Discov*. 2022;21(8):601–620. doi:10.1038/s41573-022-00470-y
33. Schilperoort M, Ngai D, Sukka SR, Avrampou K, Shi H, Tabas I. The role of efferocytosis-fueled macrophage metabolism in the resolution of inflammation. *Immunol Rev*. 2023;319(1):65–80. doi:10.1111/imr.13214
34. Jia D, Chen S, Bai P, et al. Cardiac resident macrophage-derived legumain improves cardiac repair by promoting clearance and degradation of apoptotic cardiomyocytes after myocardial infarction. *Circulation*. 2022;145(20):1542–1556. doi:10.1161/circulationaha.121.057549
35. DeBerge M, Zhang S, Glinton K, et al. Efferocytosis and outside-in signaling by cardiac phagocytes. links to repair, cellular programming, and intercellular crosstalk in heart. *Front Immunol*. 2017;8:1428. doi:10.3389/fimmu.2017.01428
36. Chuang ST, Stein JB, Nevins S, et al. Enhancing CAR macrophage efferocytosis via surface engineered lipid nanoparticles targeting LXR signaling. *Adv Mater*. 2024;36(19):e2308377. doi:10.1002/adma.202308377
37. Bamezai S, Zhang Y, Kumari M, et al. Pro-efferocytic nanotherapies reduce vascular inflammation without inducing anemia in a large animal model of atherosclerosis. *Nat Commun*. 2024;15(1):8034. doi:10.1038/s41467-024-52005-1
38. Tang C, Wang H, Guo L, et al. CpG-conjugated silver nanoparticles as a multifunctional nanomedicine to promote macrophage efferocytosis and repolarization for atherosclerosis therapy. *ACS Appl Mater Interfaces*. 2023. doi:10.1021/acsami.3c11227
39. Liu X, Ou X, Zhang T, et al. In situ neutrophil apoptosis and macrophage efferocytosis mediated by glycyrrhiza protein nanoparticles for acute inflammation therapy. *J Control Release*. 2024;369:215–230. doi:10.1016/j.jconrel.2024.03.029
40. Gao J, Pang Z, Wang Q, et al. Biomimetic nano-degrader based CD47-SIRPα immune checkpoint inhibition promotes macrophage efferocytosis for cardiac repair. *Adv Sci*. 2024;11(24):e2306388. doi:10.1002/advs.202306388
41. Zhang B, Zou Y, Tang Q, et al. SIRPα modulates microglial efferocytosis and neuroinflammation following experimental subarachnoid hemorrhage via the SHP1/STAT6 axis. *J Neuroinflammation*. 2025;22(1):88. doi:10.1186/s12974-025-03414-6
42. Ngai D, Schilperoort M, Tabas I. Efferocytosis-induced lactate enables the proliferation of pro-resolving macrophages to mediate tissue repair. *Nat Metab*. 2023;5(12):2206–2219. doi:10.1038/s42255-023-00921-9
43. Sukka SR, Ampomah PB, Darville LNF, et al. Efferocytosis drives a tryptophan metabolism pathway in macrophages to promote tissue resolution. *Nat Metab*. 2024;6(9):1736–1755. doi:10.1038/s42255-024-01115-7
44. Mahmoodzadeh S, Fliegner D, Dworatzek E. Sex differences in animal models for cardiovascular diseases and the role of estrogen. *Handb Exp Pharmacol*. 2012;(214):23–48. doi:10.1007/978-3-642-30726-3_2